Korean J. Chem. Eng., 33(5), 1571-1589 (2016)
DOI: 10.1007/s11814-015-0286-5

pISSN: 0256-1115
eISSN: 1975-7220

Increasing ethylene production as a high value hydrocarbon in Fischer-Tropsch (FT) reactor: A concept reactor for combining FT with oxidative coupling of methane

Abbas Ghareghashi*, Farhad Shahraki*, Kiyanoosh Razzaghi*, Sattar Ghader,†, and Mohammad Ali Torangi*****

*Department of Chemical Engineering, University of Sistan and Baluchestan, Zahedan 98164-161, Iran
**Department of Chemical Engineering, College of Engineering, Shahid Bahonar University of Kerman, Kerman, Iran
***Faculty of Engineering, University of Golestan, Gorgan, Iran
(*Received 7 August 2015 • accepted 16 December 2015*)

Abstract−The paper proposes a concept configuration of reactors for coupling OCM and FTS, and presents systematic simulation results. FTS section is a combination of fixed bed and membrane fluidized bed reactor, and feed of the FT reactor is supplied by OCM. The reactor configuration is compared with the consecutive reactors of OCM and one fixed bed FT reactor. Effects of CH_4/O_2 ratio, percent of N_2 in the feed, contact time, and input temperature on the yield of ethylene and valuable hydrocarbons are studied. The results show that compared with one FTS reactor configuration, the dual FTS reactor configuration is more effective and thus gives much higher product yields. Furthermore, a main decrease is observed in the formation of CO_2 and CH_4.

Keywords: Fischer-Tropsch (FT), Oxidative Coupling of Methane (OCM), C_2H_4 Yield, Fluidized Bed Reactor, Membrane Reactor

INTRODUCTION

Ethylene and its derivatives are important ingredients for industry and production of plastics, such as polyethylene. In addition, ethylene can be converted to liquid hydrocarbons, such as alpha olefins. However, ethylene in the world is produced via cracking of hydrocarbon feedstock. The feedstock is conventionally naphtha, but, nowadays, LPG and gasoline are also used. Because of the shortage of the prime feedstock, several attempts have been made to replace this feedstock with other raw materials. The oxidative coupling of methane (OCM) to produce directly ethane and ethylene (C_2 hydrocarbons) has gained great interest in the past years. Since 1982, there have been many studies on the OCM process [1]. Despite the advantages associated with the direct conversion of methane to these valuable C_{2+} hydrocarbons, low yield of this process which does not exceed 30% is the main problem [2]. Heat management, the required energy and high costs for gas separation [3] are still the prevailing problems, and attempts for commercialization of OCM process have failed. The coupling of methane without oxygen is highly endothermic and its conversion is limited due to thermodynamic limitations [4]. However, the process is exothermic in the presence of oxygen. Eq. (1) shows the overall pathway of OCM:

$$2CH_4+O_2\rightarrow C_2H_4+2H_2O \quad (1)$$
$$\Delta H_r\ (800\ ^\circ C)=-139\ kJ/mol$$

However, due to thermodynamic reasons, the partial oxidation and total oxidation are favored in the OCM process

$$CH_4+O_2\rightarrow CO+H_2O+H_2 \quad (2)$$
$$\Delta H_r\ (800\ ^\circ C)=-519\ kJ/mol$$

$$CH_4+2O_2\rightarrow CO_2+2H_2O \quad (3)$$
$$\Delta H_r\ (800\ ^\circ C)=-801\ kJ/mol$$

Consequently, catalysts are used to achieve a reasonable C_{2+} yield. The available catalysts are still little active at low temperatures. Therefore, the OCM process is performed at temperatures between 600 and 900 °C [5], which leads to lower C_{2+} yield because of the increasing CO_x formation and severe catalyst deactivation. In addition to carbon monoxide, hydrogen is also produced in OCM reactor. Fischer-Tropsch (FT) is a catalytic route for producing valuable hydrocarbons from synthesis gas. Different hydrocarbons can be produced in FT depending on temperature, pressure and catalyst. However, FT can also be a way for converting waste and by-products to hydrocarbons. Such by-products are produced in the OCM reaction.

Ehsani et al. [6] simulated the catalytic OCM reactor for ethylene production. Simulated results showed that selectivity and yield of the desired products (C_{2+}) was basically increased in the temperature range of 750-850 K. Likewise; it was observed that the GHSV has positive effect on C_{2+} selectivity. Lee et al. [7] demonstrated improved C_{2+} yield when GHSV, CH_4/O_2 ratio and reaction temperature were changed in OCM reactor system. Their simulation results showed that reactor temperature has more effect on CH_4 conversion and C_{2+} yield compared to other parameters. They found that the yield of undesirable products (CO and CO_2) can be decreased when GHSV and CH_4/O_2 ratio increases [7]. Godini et al. [8] developed a comprehensive two-dimensional model which considered the mass and heat transfer in both radial and axial directions to simulate the performance of OCM reactions in a porous packed bed membrane reactor. To investigate the relative

†To whom correspondence should be addressed.
E-mail: sattarghader@yahoo.com, sattar.ghader@gmail.com, ghader@uk.ac.ir

effects of diffusion and catalyst activity on the predicted performance of the membrane reactor, the kinetics of two different catalysts, La_2O_3/CaO and Mn-Na_2WO_4/SiO_2, was implemented in the model. The CH_4 conversion of 31.6%, low level of C_{2+} yield (25.1%), and C_{2+} selectivity of 79.5% could be obtained in membrane reactor using La_2O_3/CaO catalyst [8].

Marvast et al. [9] studied Fe-based FTS at high temperature. Their simulation results showed that the reacting gas is poor in H_2 in the second half of the reactor and adding hydrogen to the system is necessary. Ghareghashi et al. [10] investigated gasoline yield in a FT reactor in two cases of fixed bed and membrane reactor, which resulted in the increased C_{5+} yield in membrane reactor [10]. Park et al. [11] proposed a 2D heterogeneous model with fixed bed FT reactor to study the effect of tube diameter on various parameters. The simulation results showed that with an increase in reactor diameter, temperature increased in both radial and axial terms. Such an increase in temperature reduced the selectivity of the desired products and increased the yields of undesirable products [11]. Moazami et al. [12] modeled the effect of temperature and GHSV on CO conversion and production yield in a packed bed FT reactor. They concluded that raising the temperature could increase the conversion of CO, but it was undesirable because undesirable products such as methane were produced and catalyst activity was decreased. They also reported that with reduction of GHSV to 1200, CO conversion increased to 87.19% [12].

However, to produce more ethylene, carbon monoxide and hydrogen of OCM products can be used efficiently in subsequent FT reactor. It may be also useful to study subsequent FT reaction in hydrogen selective membrane fluidized bed reactor as well as fixed bed reactor. The advantages of the fluidization concept are small pressure drop, prevention of problems such as radial gradients, mass transfer limitation, and if desired high production capacity. Packed bed reactors are seriously limited by poor heat transfer and hot spot formation in the inlet of reactor.

In this study, ethylene and valuable hydrocarbons are increased by arranging reactors in a configuration of consequent OCM and FT reactors. Methane and oxygen enter the OCM reactor and produce ethylene. To produce more ethylene, CO and H_2 that are the by-products of OCM reaction are used in FT reactor to produce more ethylene. FT section is a combination of fixed bed and fluidized bed reactor. At the end of the fixed bed FT reactor, all of the hydrogen is usually consumed and no more is left for the reaction. For this reason, hydrogen permeation through the membrane into the reaction side can overcome this problem using a fluidized bed membrane reactor. The simulated results are compared with the results of consecutive reactors of OCM and fixed bed FT reactor. Finally, parametric sensitivity analysis is performed to show the effect of various parameters on the results obtained from the proposed model.

REACTION SCHEME AND KINETICS

1. Oxidative Coupling of Methane Kinetics

Kinetic model of Stanch et al. [13] is used in this study for OCM reaction. A set of nine catalytic reactions and one gas phase reaction on La_2O_3/CaO catalyst is suggested by Stanch et al. The reactions are shown below: The first three reactions involve parallel oxidation of methane. Reaction four is carbon monoxide oxidation. In the fifth reaction, ethylene is produced by ethane oxidative dehydrogenation. Part of ethylene formed from ethane might become oxidized to carbon monoxide through either reaction 6 or 8. Reactions 9 and 10 are the side reactions of water gas shift which are emphasized experimentally for many catalysts in the temperature range of 973 to 1,073 K.

Step 1: $CH_4+2O_2\rightarrow CO_2+2H_2O$ (4)

Step 2: $2CH_4+0.5O_2\rightarrow C_2H_6+H_2O$ (5)

Step 3: $CH_4+O_2\rightarrow CO+H_2O+H_2$ (6)

Step 4: $CO+0.5O_2\rightarrow CO_2$ (7)

Step 5: $C_2H_6+0.5O_2\rightarrow C_2H_4+H_2O$ (8)

Step 6: $C_2H_4+2O_2\rightarrow 2CO+2H_2O$ (9)

Step 7: $C_2H_6\rightarrow C_2H_4+H_2$ (10)

Step 8: $C_2H_4+2H_2O\rightarrow 2CO+4H_2$ (11)

Step 9: $CO+H_2O\rightarrow CO_2+H_2$ (12)

Step 1: $CO_2+H_2\rightarrow CO+H_2O$ (13)

The reaction rates for each step are given below:

$$r_j=\frac{(k_{0,j}e^{-E_{a,j}/RT}P_C^{m_j}P_{O_2}^{n_j})}{(1+K_{j,CO_2}e^{-\Delta H_{ad,CO_2,j}/RT}P_{CO_2})^2}\quad j=1,3-6 \tag{14}$$

$$r_2=\frac{k_{0,2}e^{-E_{a,2}/RT}(K_{0,O_2}e^{-\Delta H_{ad,O_2,2}/RT}P_{O_2})^{n_2}P_{CH_4}}{[1+(K_{0,O_2}e^{-\Delta H_{ad,O_2,2}/RT}P_{O_2})^n+K_{j,CO_2}e^{-\Delta H_{ad,CO_2,2}/RT}P_{CO_2}]^2} \tag{15}$$

$$r_7=k_{0,7}e^{-E_{a,7}/RT}P_{C_2H_6} \tag{16}$$

$$r_8=k_{0,8}e^{-E_{a,8}/RT}P_{C_2H_6}^{m_8}P_{H_2O}^{n_8} \tag{17}$$

$$r_9=k_{0,9}e^{-E_{a,9}/RT}P_{CO}^{m_9}P_{H_2O}^{n_9} \tag{18}$$

$$r_{10}=k_{0,10}e^{-E_{a,10}/RT}P_{CO_2}^{m_{10}}P_{H_2}^{n_{10}} \tag{19}$$

The kinetic parameters estimated for the reaction scheme presented above over La_2O_3/CaO catalyst are summarized in Table 2.

2. Fischer-Tropsch Reaction

The FT reactants include H_2 and CO which produces hydrocarbon in the following reactions taken from [14]:

Step 1: $CO+3H_2\xrightarrow{R_1}CH_4+H_2O$ (20)

Step 2: $2CO+4H_2\xrightarrow{R_2}C_2H_4+2H_2O$ (21)

Step 3: $2CO+5H_2\xrightarrow{R_3}C_2H_6+2H_2O$ (22)

Step 4: $3CO+7H_2\xrightarrow{R_4}C_3H_8+3H_2O$ (23)

Step 5: $4CO+9H_2\xrightarrow{R_5}n\text{-}C_2H_{10}+4H_2O$ (24)

Step 6: $4CO+9H_2\xrightarrow{R_6}C_4H_{10}+4H_2O$ (25)

Step 7: $6.05CO+12.23H_2\xrightarrow{R_7}C_{6.05}H_{12.36}(C_5^+)+6.05H_2O$ (26)

Step 8: $CO+H_2O\xrightarrow{R_8}CO_2+H_2O$ (27)

Table 1. Kinetic parameters of Fischer-Tropsch reactions [23]

Reaction no.	M	n	K_i	E_i (J/mol)
1	−1.0889	1.5662	142583.8	83423.9
2	0.7622	0.0728	51.556	65018
3	−0.5645	1.3155	24.717	49782
4	0.4051	0.6635	0.4632	34885.5
5	0.4728	1.1389	0.00474	27728.9
6	0.8204	0.5026	0.00832	25730.1
7	0.5850	0.5982	0.02316	23564.3
8	0.5742	0.710	410.667	58826.3

The reaction rate equations and kinetic parameters of each reaction are listed in Table 1.

$$R_i = 0.278 K_i \exp\left(\frac{-E_i}{RT}\right) P_{CO}^{m} P_{H_2}^{n} \ (\text{mol}\cdot\text{kg}_{cat}^{-1}\cdot\text{s}^{-1}) \quad (28)$$

The kinetic model is valid for the temperature, pressure, and H_2/CO ratio of 290-310 °C, 15-23 bar, and 0.76-1.82, respectively [15].

REACTOR CONFIGURATION

The first reactor in this work is OCM, in which synthesis gas

Table 2. Kinetic parameters of OCM reactions [20]

Step	$k_{0,j}$ (mol g^{-1} s^{-1} $pa^{-(m+n)}$)	$E_{a,j}$ (kJ mol^{-1})	m_j	n_j	K_{j,CO_2} (pa^{-1})	$\Delta H_{ad,CO_2}$ (kJ mol^{-1})	K_{j,O_2} (pa^{-1})	$\Delta H_{ad,O_2}$ (kJ mol^{-1})
1	0.2×10^{-5}	48	0.24	0.76	0.25×10^{-12}	−175		
2	23.2	182	1.0	0.40	0.83×10^{-13}	−186		
3	0.52×10^{-6}	68	0.57	0.85	0.36×10^{-13}	−187	0.23×10^{-11}	−124
4	0.11×10^{-3}	104	1.0	0.55	0.40×10^{-12}	−168		
5	0.17	157	0.95	0.37	0.45×10^{-12}	−166		
6	0.06	166	1.0	0.96	0.16×10^{-12}	−211		
7	1.2×10^{7a}	226						
8	9.3×10^{3}	300	0.97	0				
9	0.19×10^{-3}	173	1.0	1.0				
10	0.26×10^{-1}	220	1.0	1.0				

[a]Units are in mol s^{-1} m^{-3} pa^{-1}

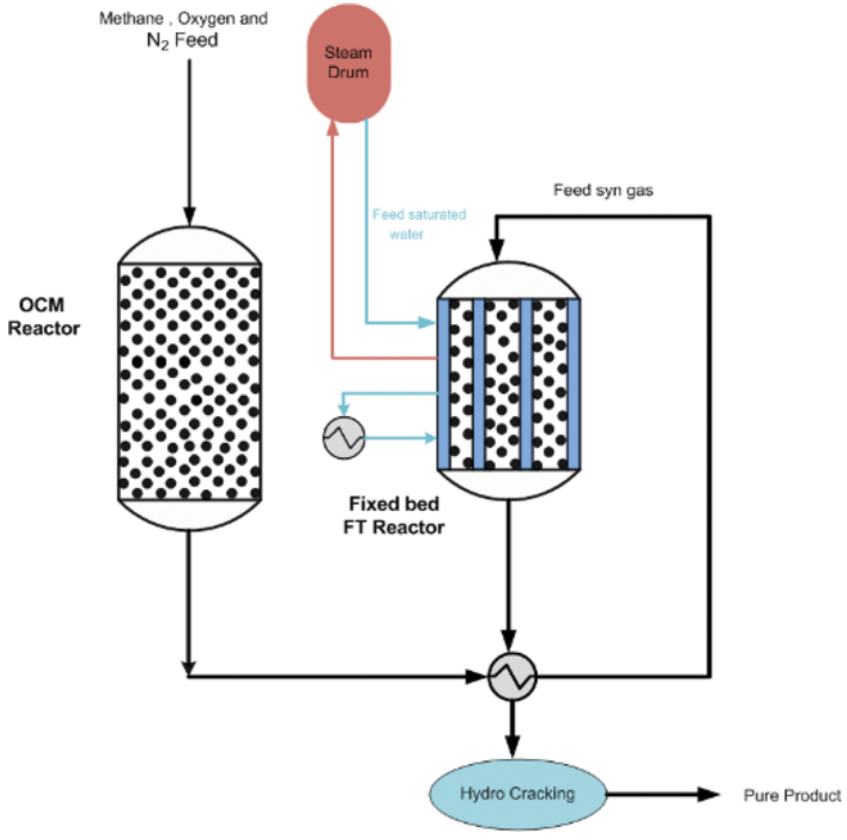

Fig. 1. Schematic diagram of OCM and FT reactors.

and C_{2+} are produced for the second reactor where CO and H_2 are converted to ethylene and heavy hydrocarbons. In another configuration, FTS is investigated in a fixed bed and fluidized bed mem-

Table 3. OCM reactor's parameters and constants [13]

Parameter	Dimension
Inner diameter (mm)	38.1
Pressure (kPa)	110
Length of catalyst bed (mm)	12000
Catalyst weight, m_{cat} (g)	0.007-1.000
Flow rate (STP), υ_{STP} ($m^3\ s^{-1}$)	4×10^{-6}-13×10^{-4}
Catalyst size (mm)	0.25-0.35
Catalyst density (kgm^{-3})	3600

Table 4. Characteristics of FTS pilot plant [16]

Parameter	Value
Tube dimension (mm)	Ø38.1×3×12 000
Feed temperature (K)	569
Cooling temperature (K)	566.2
Reactor pressure (kPa)	1700
Catalyst density (kgm^{-3})	1290
Catalyst size (mm)	Ø2.51×5.2
Bulk density (kgm^{-3})	730
Tube length (m)	12
Number of tubes	1
GHSV (h^{-1})	235
Feed molar flow rate ($gmol\ s^{-1}$)	0.0335
Bed voidage	0.488

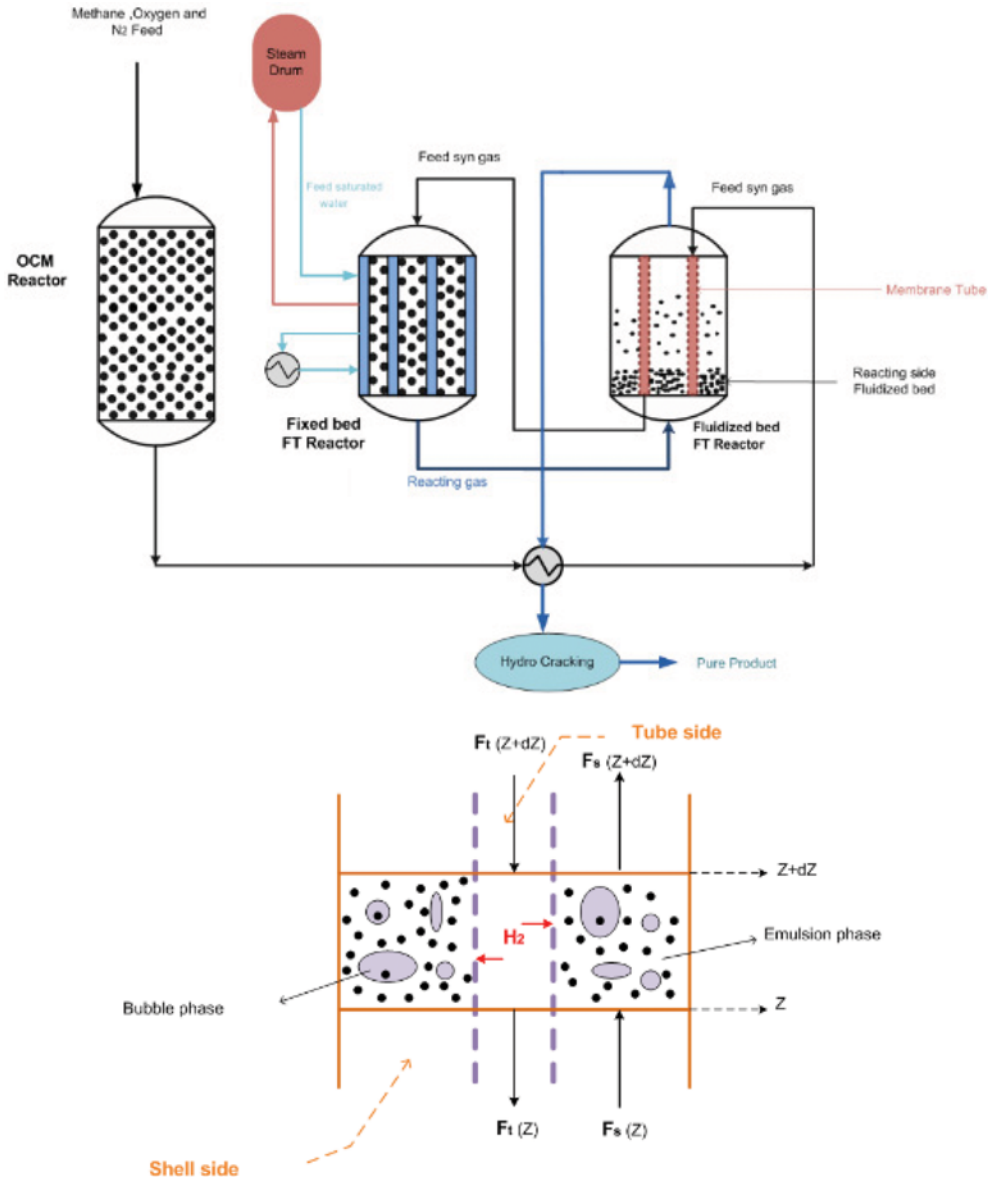

Fig. 2. (a) Figure of consecutive reactors: OCM and FT reactors (fixed bed and membrane fluidized bed in series). (b) An elemant of system for mass and energy balance equations.

brane reactor with bifunctional Fe-HZSM5 catalyst (metal part: 100 Fe/5.4 Cu/7K_2O/21SiO_2 and acidic part: SiO_2/Al_2O_3=28).

1. Two-stage Reactor Configuration (Consecutive Reactors of OCM and Fixed Bed FT Reactor)

Fig. 1 shows OCM and FT synthesis reactors. In this configuration, OCM and FT reactor are used, consequently. In the OCM reactor (first reactor), feed gas containing methane, oxygen and nitrogen as diluting component enters the reactor and produces ethane, ethylene, and by-products such as synthesis gas. Effluent gas enters the FT reactor (second reactor) and is converted to valuable hydrocarbons such as ethylene. Table 3 shows the operational conditions and dimensions of OCM reactor packed with La_2O_3/CaO. The data are derived from Stansch et al. [13]. These characteristics are used for simulation of reactor. Specifications of the fixed bed FT reactor are given in Table 4 [9].

2. Three-stage Reactor Configuration (Consecutive Reactors of OCM and Fluidized Bed Membrane FT Reactor)

Fig. 2 shows the schematic diagram of OCM (first reactor) and two consecutive reactors for FTS. In this configuration, the OCM reactor is not changed, but the performance of the fixed bed FT reactor is enhanced by the following fluidized bed reactor. In other words, this new FTS configuration is based on the two reactors consisting of a water cooled fixed bed and a synthesis gas cooled reactor. Specifications of the water cooled reactor are exactly the same as those of the previous fixed bed single stage reactor. The tubes of the fixed bed reactor and shell side of the fluidized bed reactor contain catalyst. In the fluidized bed system, the walls of the tubes consist of hydrogen perm-selective membranes, and mass and heat transfer simultaneously occur between both sides. Also, hydrogen permeation due to the hydrogen partial pressure gradient can improve the product yields.

Preheated synthesis gas enters the tubes of the fixed bed FT reactor and heat of reaction is transmitted to the available cooling water of the shell. As a result of such heat transfer, saturated water is converted to vapor and enters the steam drum. The reacting gas containing hydrocarbons leaves the fixed bed FT reactor and enters the bottom of the fluidized bed in the counter-current mode to tube synthesis gas. Catalyst characteristics and specifications of the fluidized bed membrane FT reactor are summarized in Table 5.

MATHEMATICAL MODEL

1. OCM Reactor Balance Equations

A one-dimensional heterogeneous model is assumed for OCM reactor. The system is assumed to operate in steady state condition and a plug flow fixed bed reactor model is proposed. The set of governing equations for this system is given below:

Mass balance:

$$-u_s\frac{dC_j}{dz}-\rho_b r_{c,j}+\varepsilon_b r_{g,j}=0 \tag{29}$$

Energy balance:

$$-u_s\rho_g\sum_{j=1}^{8}c_p\frac{dT}{dz}+\rho_b\sum_{j=1}^{8}r_{c,j}(-\Delta H)+\varepsilon_b\sum_{j=1}^{8}r_{g,j}(-\Delta H)-4\frac{U}{d_t}(T-T_{ex})=0 \tag{30}$$

Momentum balance (Ergun's equation):

$$-\frac{dP}{dz}=\frac{\rho_g u_s^2}{\psi d_p}\left(\frac{1-\varepsilon}{\varepsilon^3}\right)\left[\frac{150(1-\varepsilon)}{\psi Re}+1.75\right] \tag{31}$$

2. Conventional FT Reactor Balance Equations

The mathematical model of fixed bed FT reaction is developed with the assumption of one-dimensional reactor and plug flow pattern. It is also assumed that steady state condition exists and also the gas phase is ideal gas. According to the above assumptions, the mass and energy balance equations for the conventional reactor can be written as follows:

Mass balance in gas phase:

$$\frac{-F_{t0}}{A_c}\frac{dy_i}{dz}+a_v c_t k_{gi}(y_{is}-y_i)=0 \tag{32}$$

Table 5. Characteristics of FT reactors

System type	Fixed bed	Fluidized bed
Parameter	Value	Value
Tube dimension (mm)	Ø21.2×4.2×7200	Ø21.2×4.2×4800
Inner radius of Pd-Ag layer (mm)	-	0.0127
outer radius of Pd-Ag layer (mm)	-	0.01270012
Feed temperature (K)	565	-
Cooling temperature (K)	540	-
Reactor pressure (kPa)	1700	2200
Catalyst density (kgm^{-3})	1290	1290
Catalyst equivalent diameter (m)	3.83×10^{-3}	3.83×10^{-3}
Bulk density (kgm^{-3})	730	-
Tube length (m)	7.2	4.8
Number of tubes	180	16
Flow rate/tube ($gmol\ s^{-1}$)	0.0335	0.377
Catalyst thermal conductivity ($kJm^{-1}s^{-1}k^{-1}$)	0.00625	0.00625
Bed voidage	0.488	0.56 (min fluidization)

Mass balance in solid phase:

$$a_v c_t k_{gi}(y_i - y_{is}) + \rho_B \eta r_i = 0 \quad i=1, 2, \ldots, N \tag{33}$$

Energy balance in gas phase:

$$\frac{-F_{t_0}}{A_c} C_{pg} \frac{dT}{dz} + a_v h_f (T_s - T) + \frac{\pi D_i}{A_c} U_{shell} (T_{shell} - T) = 0 \tag{34}$$

Energy balance in solid phase:

$$a_v h_f (T_s - T) + \rho_B \eta \sum_{j=1}^{8} r_j (-\Delta H_{f,i}) = 0 \tag{35}$$

where y_i, T, y_s, and T_s are the mole fraction and temperature in gas phase and mole fractions on the catalyst surface and solid phase temperature, respectively.

3. Fluidized Bed Membrane FT Reactor Model

3-1. Water-cooled Reactor (First Reactor)

The model is based on the following assumptions:

(a) One-dimensional heterogeneous model;

(b) Plug flow pattern is considered;

(c) Axial dispersion of mass and heat is neglected; and

(d) The gas mixture is considered ideal gas.

According to the above assumptions and the differential element along the axial direction inside the reactor, the mole and energy balance equations are obtained. The mass and energy equations for the bulk gas phase are:

$$-\frac{f_{t0}}{A_c} \cdot \frac{dy_i}{dz} + a_v \cdot c_t \cdot k_{gi} \cdot (y_{is} - y_i) = 0 \quad i=1, 2, \ldots, N \tag{36}$$

$$-\frac{f_{t0}}{A_c} \cdot c_{pg} \cdot \frac{dT}{dz} + a_v \cdot h_f (T_s - T) + \frac{\pi \cdot D_i}{A_c} \cdot U_{shell} \cdot (T_{shell} - T) = 0 \tag{37}$$

where y_i and T are the gas phase mole fraction and temperature, respectively. The boundary conditions for the bulk phase are:

$$\text{At } z=0;\ y_i = y_{i,in},\ T = T_{in} \tag{38}$$

The mass and energy balance equations for the catalyst pellets:

$$k_{gi} \cdot a_v \cdot c_t \cdot (y_i - y_{is}) + \rho_B \cdot \eta \cdot r_i = 0 \quad i=1, 2, \ldots, N \tag{39}$$

$$a_v \cdot h_f \cdot (T - T_s) + \eta \cdot \rho_B \cdot \sum_{j=1}^{8} r_j \cdot (-\Delta H_{fj}) = 0 \tag{40}$$

where y_{is} and T_s are the mole fractions on the catalyst surface and solid phase temperature, respectively. The mass transfer coefficients between the gas and solid phases are taken from Cusler [16]:

$$k_{gi} = 1.17 Re^{-0.42} Sc_i^{-0.67} u_g \times 10^3 \tag{41}$$

$$Re = \frac{2 R_p u_g}{\mu} \tag{42}$$

$$Sc_i = \frac{\mu}{\rho \cdot D_{im} \cdot 10^{-4}} \tag{43}$$

The diffusivity of each component in the gas mixture is given by [17]:

$$D_{im} = \frac{1 - y_i}{\Sigma_{i \neq j} y_i D_{ij}} \tag{44}$$

$$D_{ij} = \frac{10^{-7} \cdot T^{3/2} \sqrt{\frac{1}{M_i} + \frac{1}{M_j}}}{P\left(\theta_{ci}^{3/2} + \theta_{cj}^{3/2}\right)^2} \tag{45}$$

Table 6. Molecular weight and critical volume of the components

Component	M_i (g/mol)	v_{ci} (m^3/mol)×10^6
C_{5+}	85.084	370
i-C_4H_{10}	58.123	262.7
n-C_4H_{10}	58.123	255
C_3H_8	44.096	200
C_2H_6	30.07	145.5
C_2H_4	28.054	129.1
CO_2	44.01	94.0
CO	28.01	18.0
H_2O	18.02	56.0
H_2	2.02	6.1
CH_4	16.04	99.0
N_2	28.01	18.5

where D_{ij} is the binary diffusivity calculated using the Fuller-Schetter-Giddins equation [18]. M_i and υ_{ci} are the molecular weight and critical volume of component i which are reported in Table 6. The overall heat transfer coefficient between the circulating boiling water of the shell side and the bulk of the gas phase in the tube side is given by the following correlation:

$$\frac{1}{U_{shell}} = \frac{1}{h_i} + \frac{A_i \cdot \ln \frac{D_o}{D_i}}{2\pi L K_w} + \frac{A_i}{A_o} \cdot \frac{1}{h_o} \tag{46}$$

where h_i is the convection heat transfer coefficient between the gas phase and the reactor wall, obtained by the following correlation [18]:

$$\frac{h_i}{c_p \rho \mu} \cdot \left(\frac{c_p \cdot \mu}{k}\right)^{2/3} = \frac{0.458}{\varepsilon_B} \cdot \left(\frac{\rho \cdot u \cdot d_p}{\mu}\right)^{-0.407} \tag{47}$$

ε_B is the void fraction of the catalytic bed and d_p is the equivalent catalyst diameter. The other parameters are related to the bulk gas phase. To calculate the heat transfer coefficient of boiling water on the shell side at high pressure, Leva correlation is used [18]:

$$h_0 = 282.2 p^{4/3} \cdot \Delta T^2 \qquad 0.7 < P < 14 \text{ MPa} \tag{48}$$

3-2. Gas-cooled Reactor (Fluidized-bed Reactor)

3-2-1. Tube Side (Feed Synthesis Flow)

Assuming constant molar flow rate in the tube side, the mass and energy balance equations for the fluid phase are given as follows:

Mass balance equation:

$$\frac{f_{t0}}{A_c} \cdot \frac{dy_h}{dz} + \frac{\alpha_H}{A_s} \left(\sqrt{P_H^t} - \sqrt{P_H^{sh}}\right) = 0 \tag{49}$$

$$\alpha_H = \frac{2\pi L \bar{p}}{\ln \frac{R_o}{R_i}} \tag{50}$$

P_H^t and P_H^{sh} are the hydrogen partial pressure in the tube and shell sides, respectively. α_H is the hydrogen permeation rate constant. R_o and R_i are the outer and inner radii of Pd-Ag layer [19]. Hydrogen permeability through Pd-Ag layer is defined as a function of temperature using Arrhenius law [20]:

Table 7. Comparison of model and experimental data of [15]

	Runs					
	1023 K	1073 K	1103 K	973 K	1023 K	1103 K
Feed mole fraction						
CH_4	0.612	0.612	0.612	0.699	0.699	0.699
O_2	0.051	0.051	0.051	0.095	0.095	0.095
N_2	0.337	0.337	0.337	0.206	0.206	0.206
CH_4 conversion (%)						
Experimental data	4.9	7.9	9.9	4.1	7.1	14.4
Model	4.73	8.41	10.8	3.15	6.18	14.45
Error (%)	3.47%	6.46%	9.1%	23.17%	1.13%	0.35%
C_{2+} selectivity (%)						
Experimental data	55.6	69.2	72.5	35.6	53.7	69.6
Model	57.25	64.99	65.21	38.41	50.98	59.75
Error (%)	2.97%	6.08%	10.06%	7.89%	5.07%	14.15%
C_{2+} yield (%)						
Experimental data	2.7	5.5	7.2	1.5	3.8	10
Model	2.7	5.5	7.4	1.21	3.15	8.63
Error (%)	0%	0%	2.78%	19.3%	17.11%	13.7%

$$\overline{p} = p_0 \cdot \exp\left(\frac{-E_p}{RT}\right) \quad (51)$$

The pre-exponential factor P_0 above 200 °C is reported as 6.33×10^{-8} mol $m^{-2}s^{-1}pa^{-1/2}$ and activation energy E_p is 91270 kJ/kmol [21].

Energy balance equation:

$$\frac{f_{t0}}{A_c} c_{pgt} \frac{dT_t}{dz} + \frac{\alpha_H}{A_s}\left(\sqrt{P_H^t} - \sqrt{P_H^{sh}}\right) c_{ph}(T - T_t) - \frac{\pi D_i}{A_c} U_{tube}(T - T_t) = 0 \quad (52)$$

T_t and T indicate the synthesis gas temperature in tube side and the reacting gas temperature in shell side, respectively. The boundary conditions are as follows:

$$\text{At } z=L;\ y_i = y_{if},\ T = T_f \quad (53)$$

3-2-2. Shell Side (Reaction Side)

In this work, the fluidized bed is in the bubble regime. The two-phase theory that contains the bubble and emulsion phases is used for this regime. In two-phase theory, flow rate of the bubble phase is equal to the required residual gas flow to make minimum fluidization. Velocity of bubbles (u_b) is assumed to be constant all over the bed [22]. Thus, when bubbles rise in a fluidized bed, the dense (emulsion) phase continues to transfer gas to the rising bubbles, which in turn causes the bubbles to grow in size and rise with higher velocities [23].

In fluidized bed systems, a macro-scale circulation flow pattern with downward emulsion flow near the walls and an upward flow in the middle of the bed is dominant [16]. Accordingly, the reactor shows almost plug flow behavior.

The shell side's main assumptions are as follows:

a) Gas phase is ideal;

b) Radial distribution of concentration is negligible;

c) The bubble phase gas regime is plug;

d) Due to rapid mixing, the operation is assumed to be isothermal, which means bubble and emulsion phases have the same temperature;

e) Hydrogen is only added to the emulsion phase;

f) Gas flow through the emulsion phase remains constant at minimum fluidization velocity;

g) Given the small size of the catalyst, the diffusional resistance inside the catalyst particles is neglected;

h) Catalyst particles can be found in bubble phase and components can react in rising bubbles, too. But, the extension of chemical reactions in bubble phase is much less than emulsion phase; and

i) The axial diffusion of hydrogen through the membrane is neglected compared to the radial diffusion.

Bubble phase mass conservation equation:

$$-\delta \frac{f_t}{A_{shell}} \frac{dy_{ib}}{dz} + \delta k_{bei} c_t a_b (y_{ie} - y_{ib}) + \delta\gamma\rho_p \sum_{j=1}^{8} r_{bij} = 0 \quad (54)$$

Table 8. Comparison of CR model results with pilot plant data [13]

Parameter	Pilot plant data	Model	Error (%)
X_{CO} (%)	77.94	77.19	0.96%
X_{H_2} (%)	92.83	94.5	1.8%
CO_2 selectivity	339.07	317.32	6.4%
CH_4 selectivity	44.15	44.65	1.1%
H_2O selectivity	120.67	115.19	4.5%
C_2H_4 selectivity	3.95	3.52	1.1%
C_2H_6 selectivity	11.78	13.93	18.25%
C_3H_8 selectivity	9.33	6.42	31.19%
n-C_4 selectivity	11.07	9.65	12.82%
i-C_4 selectivity	14.45	12.23	15.36%
C_5 selectivity	42.55	45.64	7.3%

i=1, 2, …, N

Emulsion phase mass conservation equation:

$$-(1-\delta)\frac{f_t}{A_{shell}}\frac{dy_{ie}}{dz}+(1-\delta)\rho_e\eta\sum_{j=1}^{8}r_{ij}+\delta k_{bei}a_b c_t(y_{ib}-y_{ie})+(1-\delta)\frac{\alpha_H}{A_s}(\sqrt{P_H^t}-\sqrt{P_H^{sh}})=0 \quad (55)$$

y_{ib} and y_{ie} refer to the mole fraction of each component in bubble and emulsion phases, respectively. K_{bei} is the mass transfer coefficient between the bubble phase and emulsion phase, and γ is volume fraction of catalyst bed occupied by solid particles in bubble phase. A_{shell} is the area around each tube.

The heat balance equation between the shell and tube of the gas cooled reactor is:

$$-(1-\delta)\frac{\alpha_H}{A_s}(\sqrt{P_H^t}-\sqrt{P_H^{sh}})c_{pH}(T-T_t)+(1-\delta)\eta\rho_e\sum_{j=1}^{8}r_j(-\Delta H_{fj}) \quad (56)$$

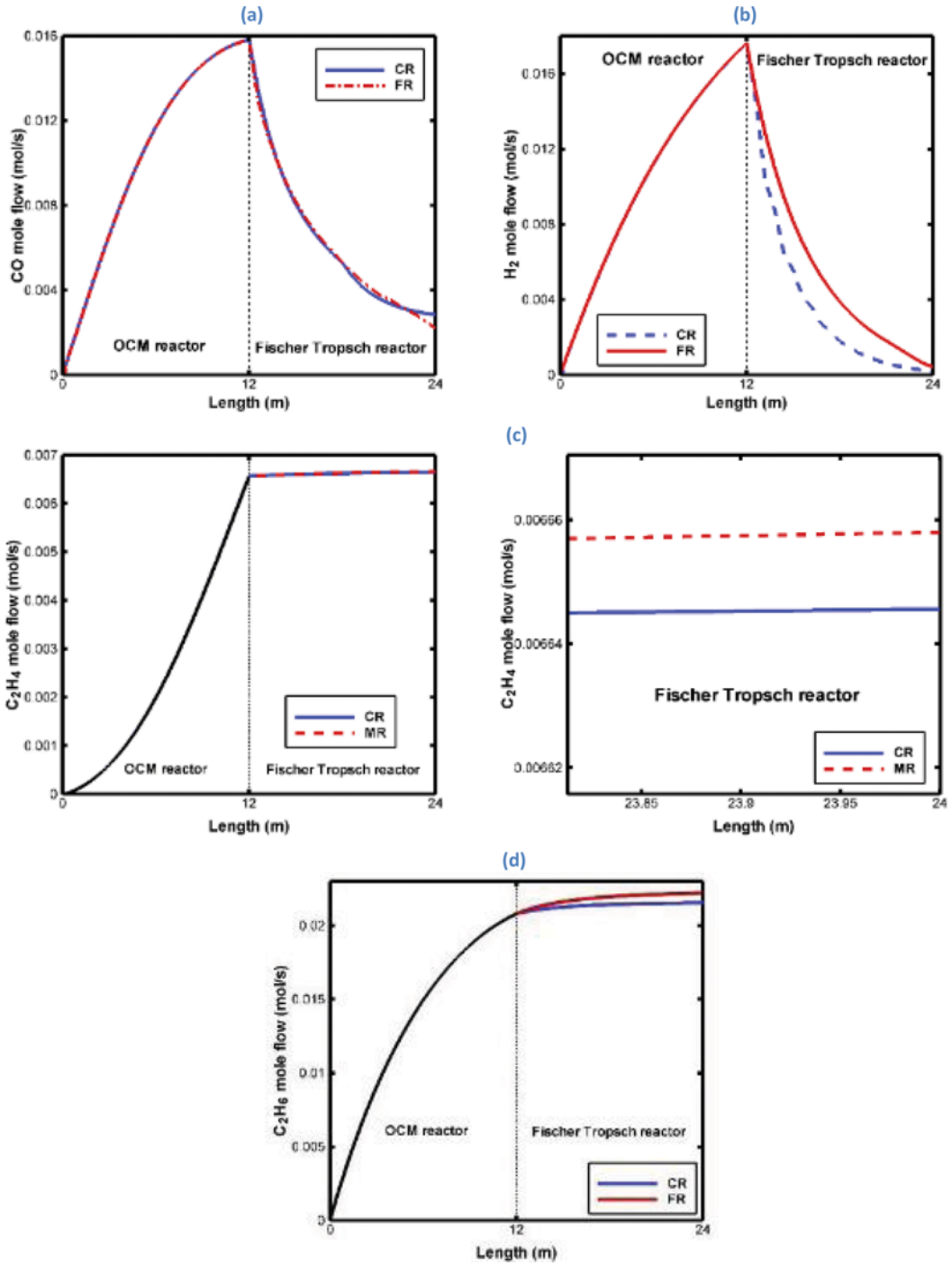

Fig. 3. Variation of CO, H_2, C_2H_4 and C_2H_6 mole flow (a)-(d) in OCM and FT reactors (in CR (conventional fixed bed) and dual type FT in series (FR)) (CH_4/O_2=12, T=1,103 K).

$$+\gamma\rho_B\sigma\eta\sum_{j=1}^{8} r_{bj}(-\Delta H_{fj})+\frac{\pi\cdot D_i}{A_{shell}}U_{shell}(T-T_t)=0$$

when α_H is zero the membrane is not permeable to hydrogen.

The empirical correlations for the hydrodynamic parameters used in the model are taken from the related literature, although they were originally obtained for the beds without internals. Based on two-phase theory, Harrison and Davidson suggested the following correlation for the velocity of rise of bubbles [24]:

$$u_b=u_0-u_{mf}+0.711(g\cdot d_b)^{0.5} \quad (57)$$

The following correlation is selected for minimum fluidization velocity [22]:

$$u_{mf}=\left(\frac{\mu_g}{\rho_g\cdot d_p}\right)\cdot\left(\sqrt{27.2^2+0.0408Ar}-27.2\right) \quad (58)$$

where Ar is Archimedes number.

To calculate the bubble diameter at each height of bed, the following correlation is used [24]:

$$d_b=0.00853(1+0.272(u_0-u_{mf}))^{1/3}\cdot(1+0.0684z)^{1.21} \quad (59)$$

The mass transfer coefficient between the bubble and emulsion phases in fluidized bed reactor is [25]:

$$k_{be}=0.75u_{mf}+\left(\frac{g\cdot D_m^2}{d_b}\right)^{0.25} \quad (60)$$

where D_m is the diffusivity of each component in the gas mixture.

The heat transfer coefficient between the bubble and emulsion phases in fluidized bed reactor is:

$$h=h_g+h_r+(1-\delta)\left(\frac{2k_{ew}^0}{d_p}+0.05c_{pg}\cdot\rho_g\cdot u_0\right) \quad (61)$$

where h_g and h_r are convection and radiation heat transfer coefficients, respectively, and k_{ew}^0 is the effective heat conduction of a bed thin layer near the wall surface.

SIMULATION AND DISCUSSION

1. Model Validation

The ability of the models to estimate the results of FT and OCM reactors is tested by comparing the predictions with the experimental data. OCM model validation is carried out by the comparison of model calculation with the experimental results by Stansch et al. on La_2O_3/CaO catalyst [13]. Table 7 presents the results of simulation and experimental data for OCM reactor under the same conditions and the actual reactor dimension in two different feed ratios. At high methane to oxygen ratio, model shows good agree-

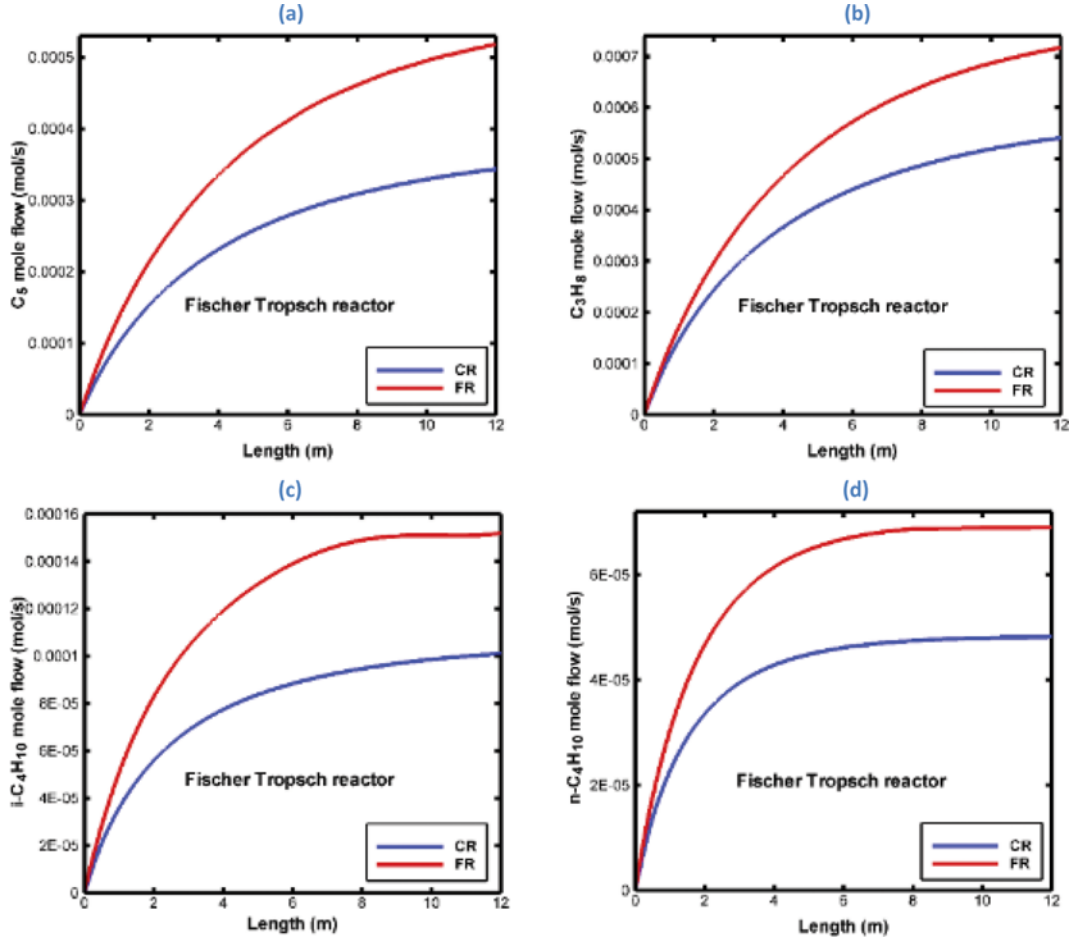

Fig. 4. Variation of C_5, C_3H_8, i-C_4H_{10}, and n-C_4H_{10} mole flow (a)-(d) in FT reactors (in CR and dual type reactors) (CH_4/O_2=12, T=1,103 K).

ment with experimental data, but in the second one low agreement is obtained, and at lower temperatures the error is even 19%. The reason for this error could be neglecting of reactions in the areas of pre-catalytic and post-catalytic in modeling calculations. In these areas, gas phase reactions such as oxidation and thermal decomposition reactions occur. However, both OCM and FT processes have significant scaling up effects and the usage of the kinetic data from literature should be performed with caution. FT reactor is validated by comparing its results with the experimental data of RIPI pilot plant [15] in Table 8. As can be seen, there is good agreement between experimental data and simulation results for CO and H_2 conversion and C_5 selectivity. However, for ethane, propane and butane selectivity some deviation can be seen. The deviation of the simulated selectivity of propane from the experimental result

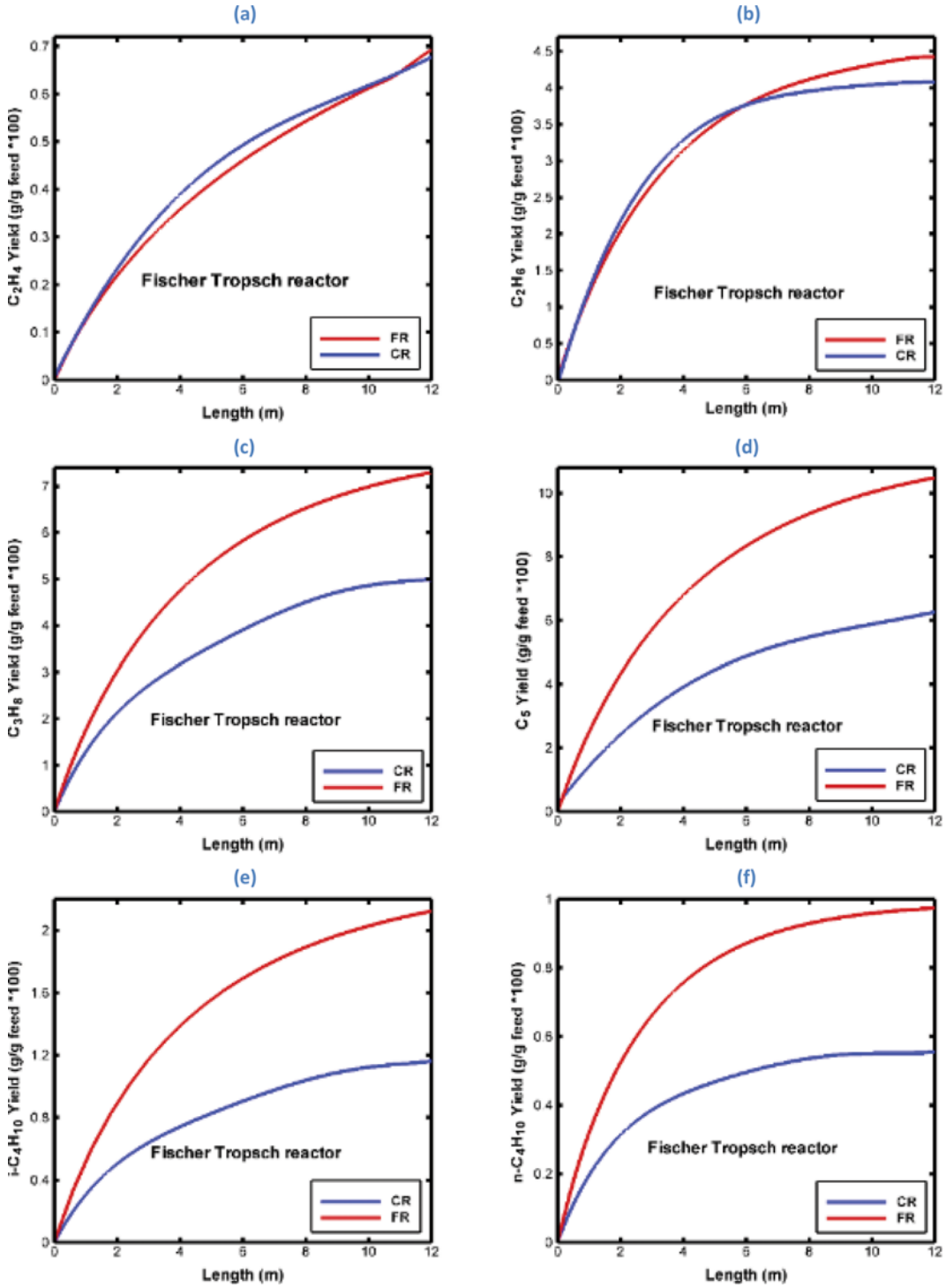

Fig. 5. Variation of (a) C_2H_4 (b) C_2H_6 (c) C_3H_8 (d) C_5 (e) i-C_4H_{10} (f) n-C_4H_{10} (g) CH_4 (h) CO_2 yield in CR and FR reactors (CH_4/O_2=12, T= 1,103 K).

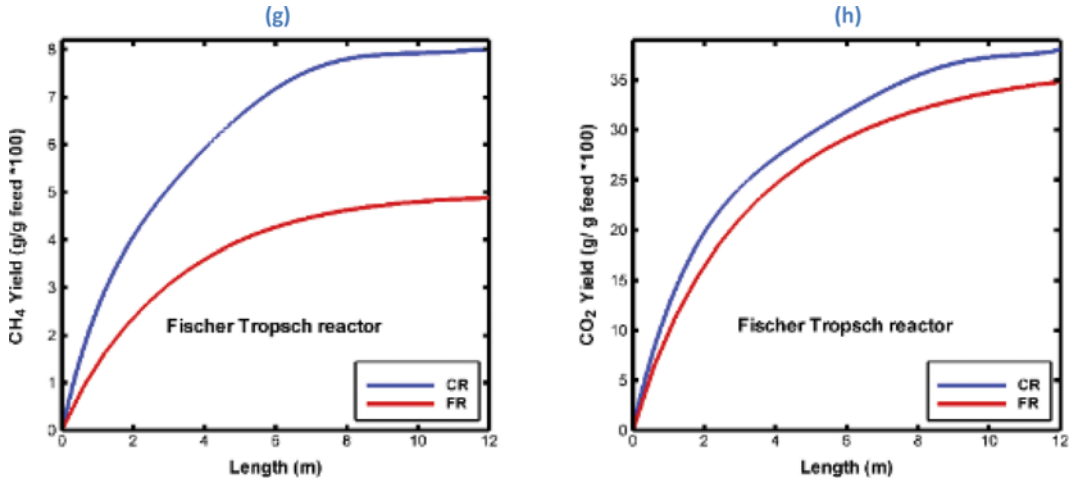

Fig. 5. Continued.

is as high as 31.19%. However, the kinetic model did not consider the effect of secondary reactions of alpha olefins such as readsorption, hydrogenation and isomerization, which might lead to some deviation in results. Readsorption is based on hypothesis that linear alpha olefin readsorb on the active sites and can initiate the chain growth.

2. Simulation Results

2-1. Component Mole Flow and Product Yield in Length of Reactor

Results of OCM and FT reactor models are shown in Figs. 3(a)-(d). Mole flow of ethylene, ethane, hydrogen and carbon monoxide in OCM and FT reactors is compared in two configurations: fixed bed FT reactor (denoted by CR) and dual type FT reactor (denoted by FR). Use of membrane reactor has positive effect. As shown in Figs. 3(a) and (b), hydrogen mole flow in dual type system is higher than conventional system due to adding hydrogen to the reaction side through Pd-Ag membrane. Furthermore, diffusion of hydrogen promotes the conversion of carbon monoxide. Figs. 3(c) and (d) show that mole flow of ethylene and ethane in FR reactor increases in comparison to CR reactor; in fact, hydro-

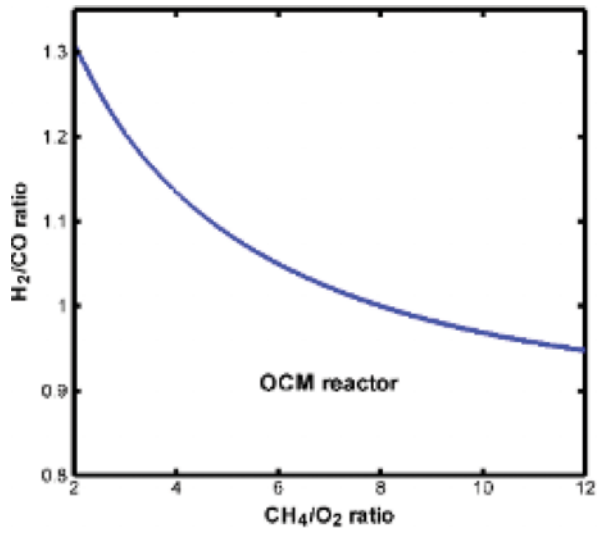

Fig. 6. Variation of H_2/CO ratio produced in OCM reactor as a function of CH_4/O_2 ratio (T=1,103 K, N_2 mole fraction=0.337).

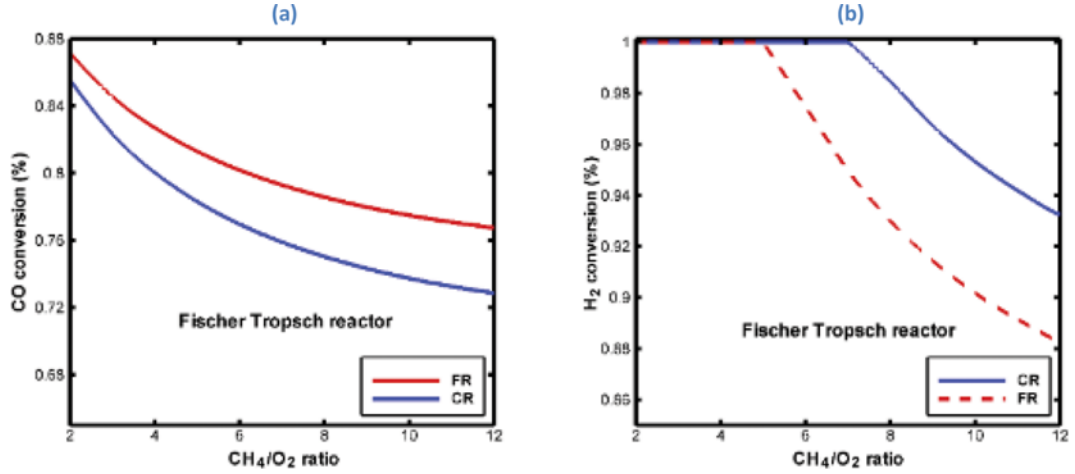

Fig. 7. Effect of CH_4/O_2 ratio in OCM reactor feed on (a) CO conversion and (b) H_2 conversion (b) in CR and FR reactors (T=1,103 K, N_2 mole fraction=0.337).

gen permeation in the shell side improves ethylene production. In other words, the FR overcomes mass transfer limitations due to small particle size, and also controls the addition of hydrogen through the membrane. Hydrogen consumption in the water cooled reactor of FR and also in the first half of CR is relatively high. Therefore, there will be a lack of hydrogen in the second section of these reactors and adding hydrogen in FR configuration leads to more conversion of hydrogen and CO, and as a result, more hydrocarbons are produced.

Figs. 4(a)-(d) show the mole flow of hydrocarbon products such as propane, n-butane, iso-butane, and gasoline, respectively. It is clear that the dual type FT reactor enhances the formation of prod-

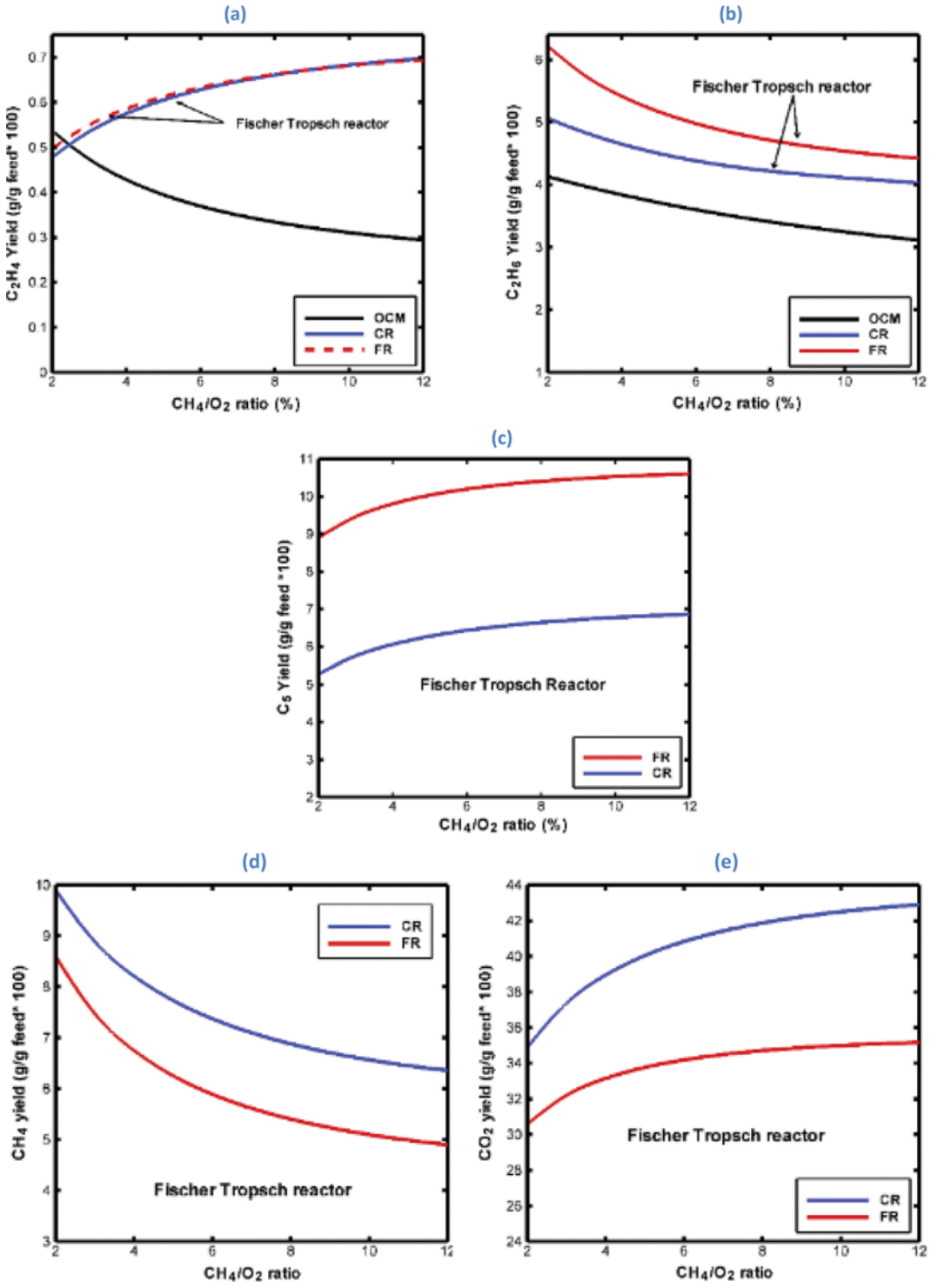

Fig. 8. Effect of CH_4/O_2 ratio in OCM reactor feed on (a) C_2H_4 (b) C_2H_6 (c) C_5 (d) CH_4 (e) CO_2 yield in CR and FR modes of FT reactor (T= 1,103 K, N_2 mole fraction=0.337).

ucts. Yield of products such as ethylene, ethane, propane, gasoline, iso-butane, n-butane, methane and carbon dioxide in FR and CR reactors is shown in Figs. 5(a)-(h). It is evident that a dual type FR reactor operates better due to decreasing production of carbon dioxide and methane as undesired by-products. Diffusion of hydrogen toward the reaction side affects the water gas shift reaction, which is desirable due to consuming CO_2.

2-2. Effect of CH_4/O_2 Ratio in OCM Feed

Figs. 6-8 represent the effect of composition of input feed of OCM reactor on the products conversion and yield. Fig. 6 indicates that with increasing CH_4/O_2 ratio, H_2/CO ratio at the end of OCM reactor decreases. Changing this ratio affects the yield of products in FT reactor. As can be seen in Fig. 7, H_2 conversion in dual type FR is less than the conventional reactor, and as a result of H_2 diffusion, more CO conversion is observed. Fig. 8 presents the change of (a) C_2H_4, (b) C_2H_6, (c) C_5, (d) CH_4 and (e) CO_2 yield with CH_4/O_2 ratio. According to Figs. 8(a) and (b), with increasing CH_4/O_2 ratio, C2 yield reduces at the outlet of OCM reactor because of insufficient oxygen in the reaction. Due to the increase of CO in the output of the OCM reactor, ethylene yield increases and also less ethane yield is observed. In the FT reaction kinetics, order of C_2H_4 is positive and change in CH_4/O_2 ratio promotes C_2H_4 production.

According to Fig. 8(c), the gasoline yield in FR is higher than CR. As demonstrated in Figs. 8(d) and (e), due to methane and carbon dioxide reaction order in FT kinetics, the yield of CH_4 decreases and yield of CO_2 increases with increasing CH_4/O_2 ratio and more CO production but their yield decreases in FR compared to CR.

2-3. Effect of N_2 Percentage in OCM Feed as an Inert Gas

Effect of inert gas in the feed of OCM reactor on H_2/CO ratio, CO and H_2 conversion and hydrocarbons yield is shown in Figs. 9-11. Changing percent of inert gas in the input feed has great effect on the yield of products in FT reactor and conversion of reactants. In the OCM reactor, inert gas is used for the dilution of input feed and reduces the temperature of reaction by capturing heat of reaction. However, reducing percent of oxygen (with diluting inert) favors oxidative coupling reactions and further prevents

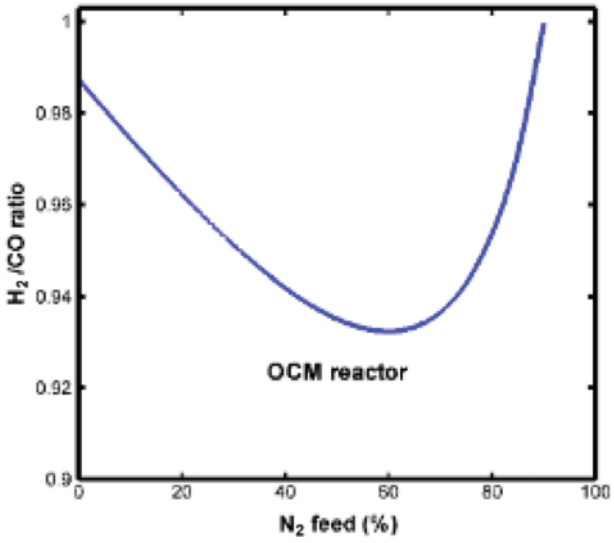

Fig. 9. Variation of H_2/CO ratio produced in OCM reactor as a function of N_2% in feed of OCM reactor (CH_4/O_2=12, T=1,103 K).

deep oxidation reaction. According to these Figs., increase in the mole of CO at 60% inert gas causes improvement of desirable products and decreases the undesired products (Fig. 11).

2-4. Temperature Profile in FT and OCM Reactors

Fig. 12 shows the gas phase temperature in the OCM and FT reactors. There are two temperature peaks in the zones close to the entrance of FR and CR reactors. For simulation purposes, the maximum temperature for the Fe-HZSM5 catalyst to remain active is assumed to be 620 K [9]. As shown in Fig. 12(a), most of the reaction heat is captured in the FR section. However, FR operates far from hotspot and temperature control is easier.

2-5. Effect of Contact Time

Fig. 13 shows the production yield of C_2H_4 in CR and FR modes and also H_2/CO ratio in OCM reactor as a function of contact time. Reactants of OCM reactor would have longer contact time with low space velocity. As a result, the reaction would go to completion and the process will be enhanced. As shown in Fig. 13(a), $H_2/$

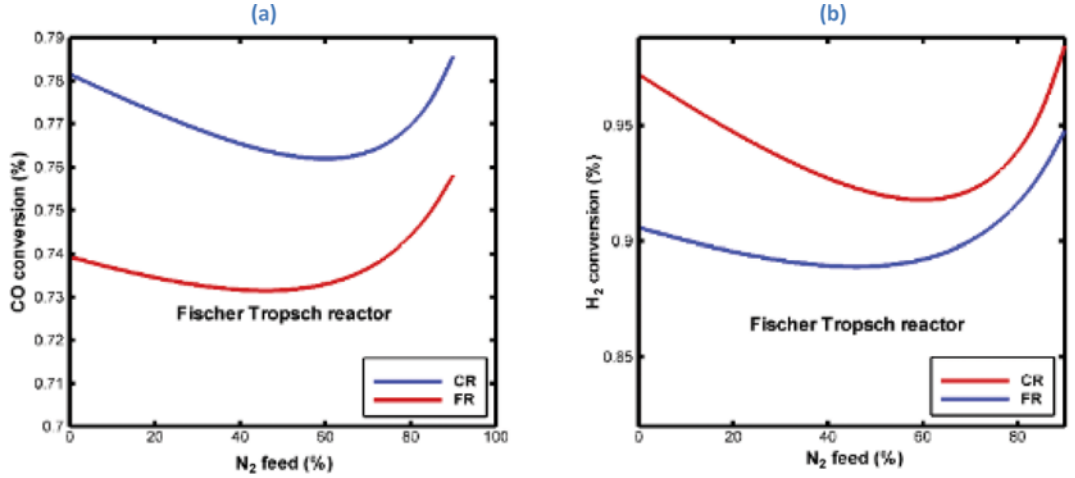

Fig. 10. Effect of N_2 % in OCM reactor feed on (a) CO conversion and (b) H_2 conversion in CR and FR reactors (CH_4/O_2=12, T=1,103 K).

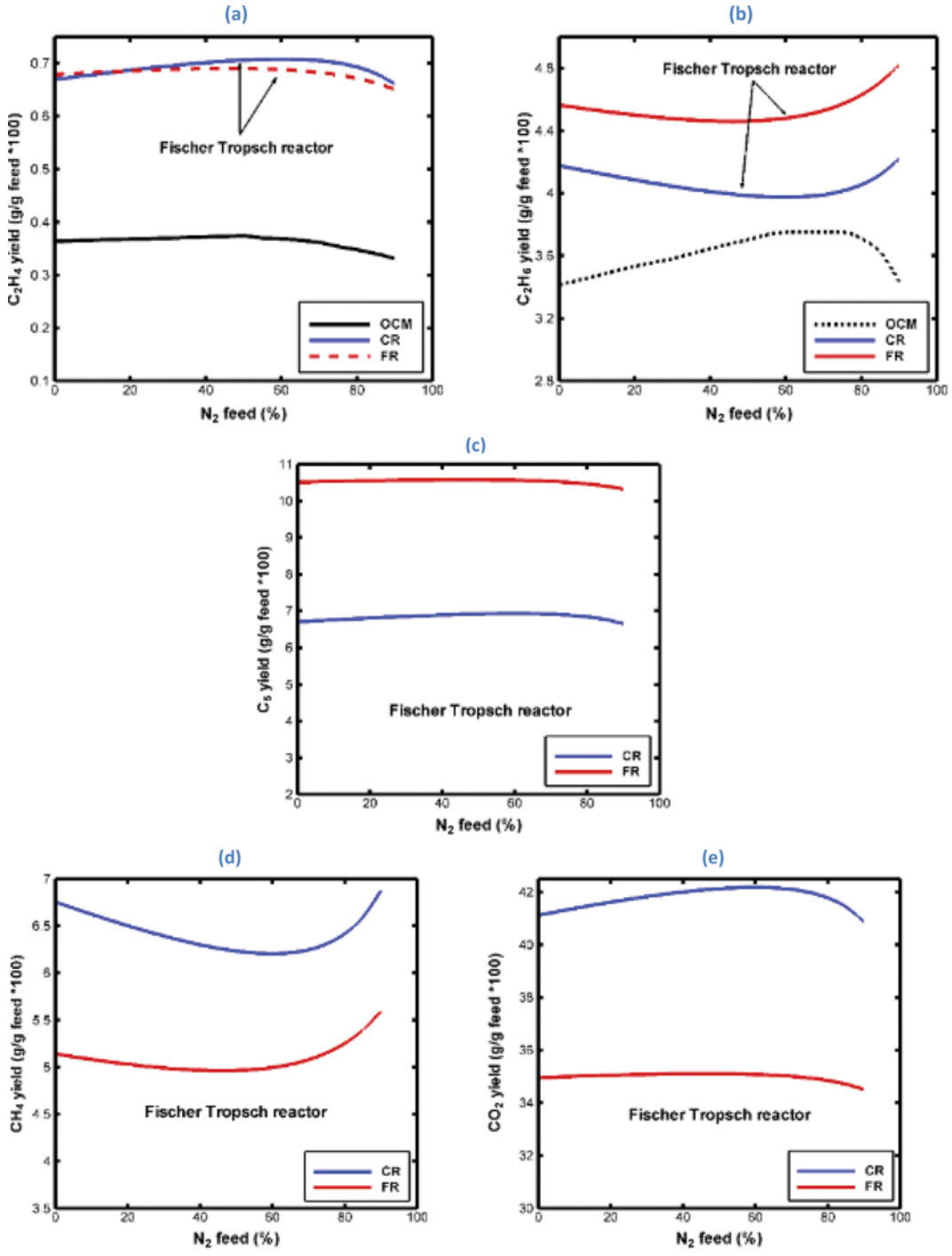

Fig. 11. Variation of (a) C_2H_4 (b) C_2H_6 (c) C_5 (d) CH_4 (e) CO_2 yield in CR and FR of FT reactor and OCM reactor as a function of N_2 % in OCM reactor feed (CH_4/O_2=12, T=1,103 K).

CO ratio decreases with the increase of contact time.

2-6. Effect of Cooling Water Temperature

Fig. 14 shows the effect of cooling water temperature on the yield of (a) C_2H_4 and (b) C_{5+} in dual type FT reactor with variation of CH_4/O_2 ratio in the inlet of OCM reactor. Increasing the cooling water temperature increases C_2H_4 yield and decreases C_{5+} yield.

2-7. Effect of FT Pressure

Fig. 15 demonstrates the reactor system performance at different pressures. With assuming that operating pressure of fixed bed FT reactor is equal to that of fluidized bed membrane FT reactor, Fig. 15 indicates that by increasing pressure of dual type FT reactor mole flow of gasoline increases. However, pressure does not have an appreciable effect on ethylene. The reason for this behavior is of partial pressure difference of hydrogen and rate of gasoline production that is more sensitive to hydrogen's partial pressure (Eq. (28)).

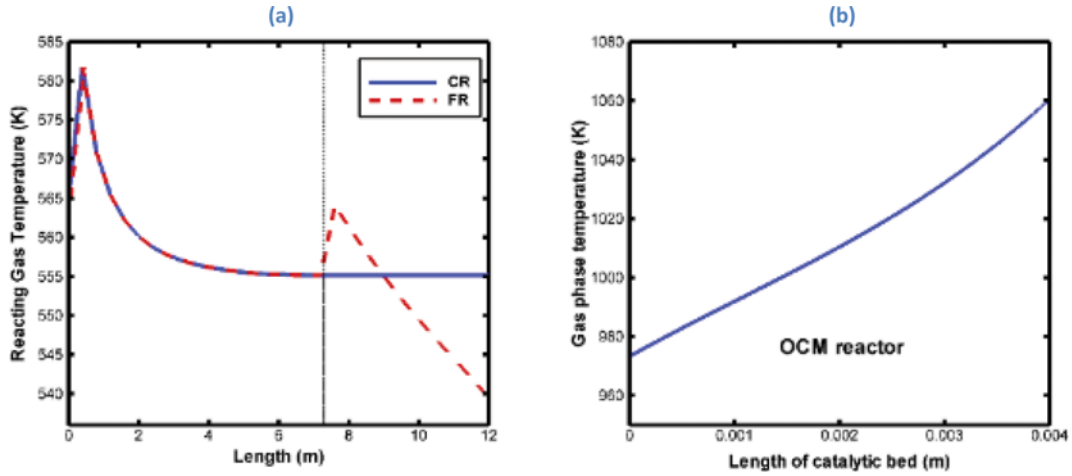

Fig. 12. Temperature profile in OCM and FT reactors.

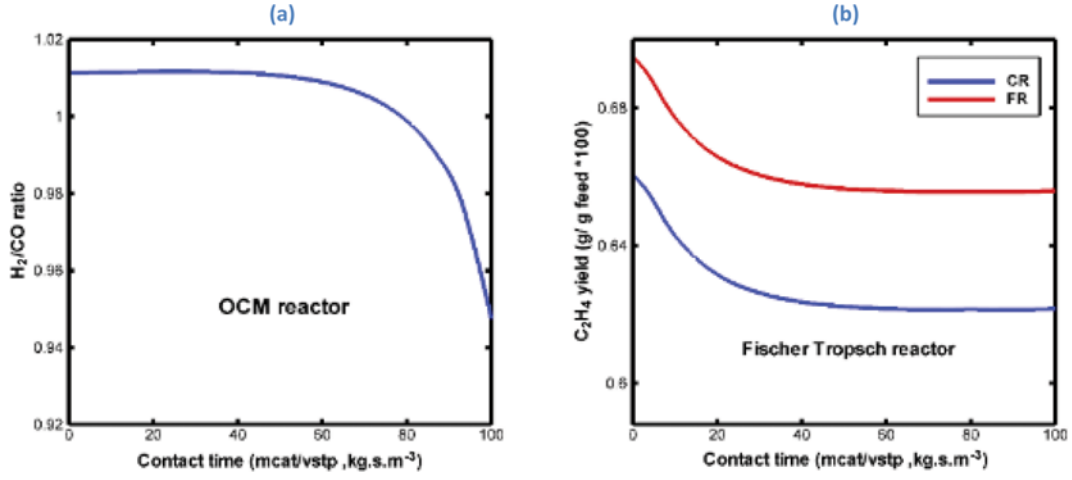

Fig. 13. Effect of contact time on (a) H_2/CO ratio in feed synthesis gas (exit of OCM reactor) (CH_4/O_2=12, T=1,103 K).

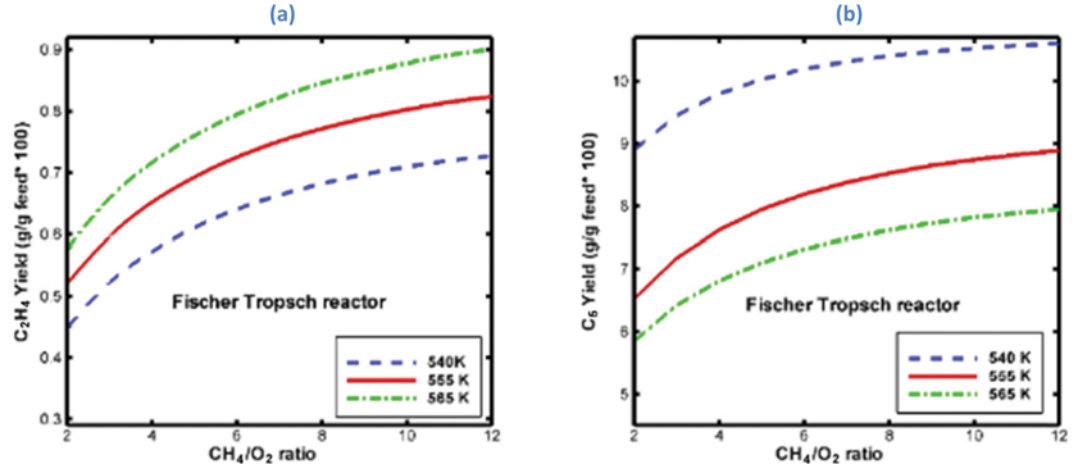

Fig. 14. Effect of cooling water temperature on (a) C_2H_4 and (b) C_{5+} yield with input CH_4/O_2 ratio in OCM.

2-8. L_{ratio} Effect of FT with Different CH_4/O_2 Ratio in OCM

Fig. 16 demonstrates the variation of (a) hydrogen conversion, yield of (b) C_2H_4, (c) CO_2 and (d) C_2H_6 with CH_4/O_2 ratio at the inlet of OCM reactor in different ratios of dual type FT reactor lengths. The ratio is defined as $L_{ratio}=(L_1/L_2)$, where L_1 and L_2 are length of fixed bed and fluidized bed membrane reactor, respec-

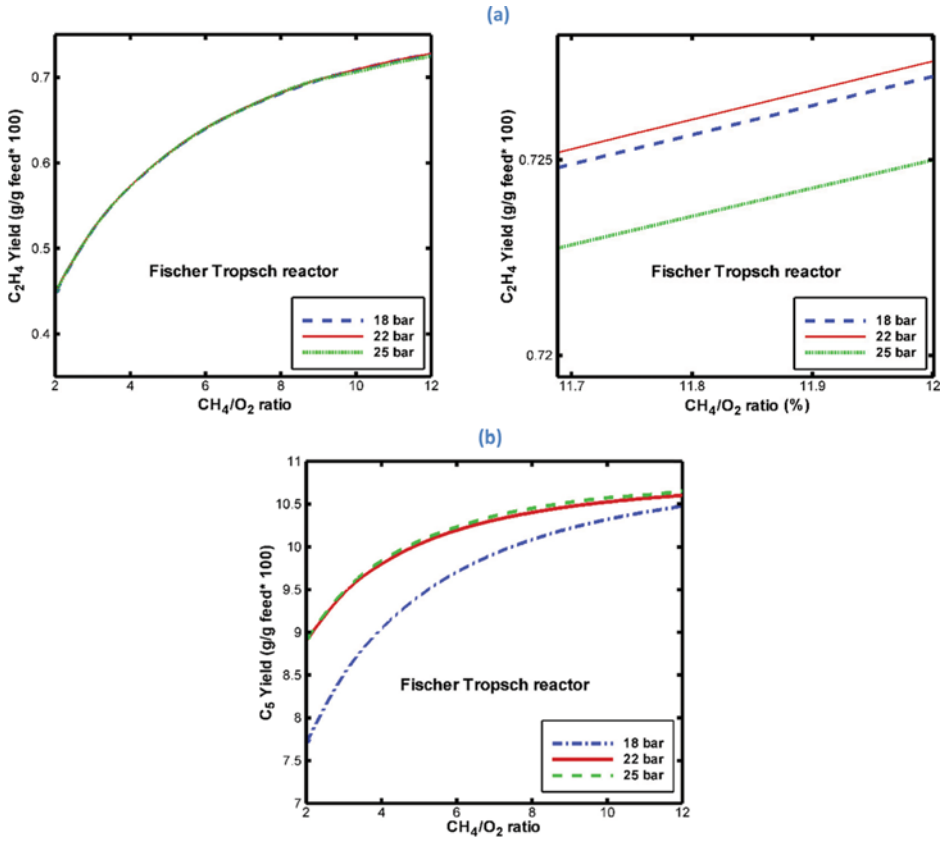

Fig. 15. Effect of pressure on (a) C_2H_4 yield and (b) C_{5+} yield with input CH_4/O_2 ratio in OCM.

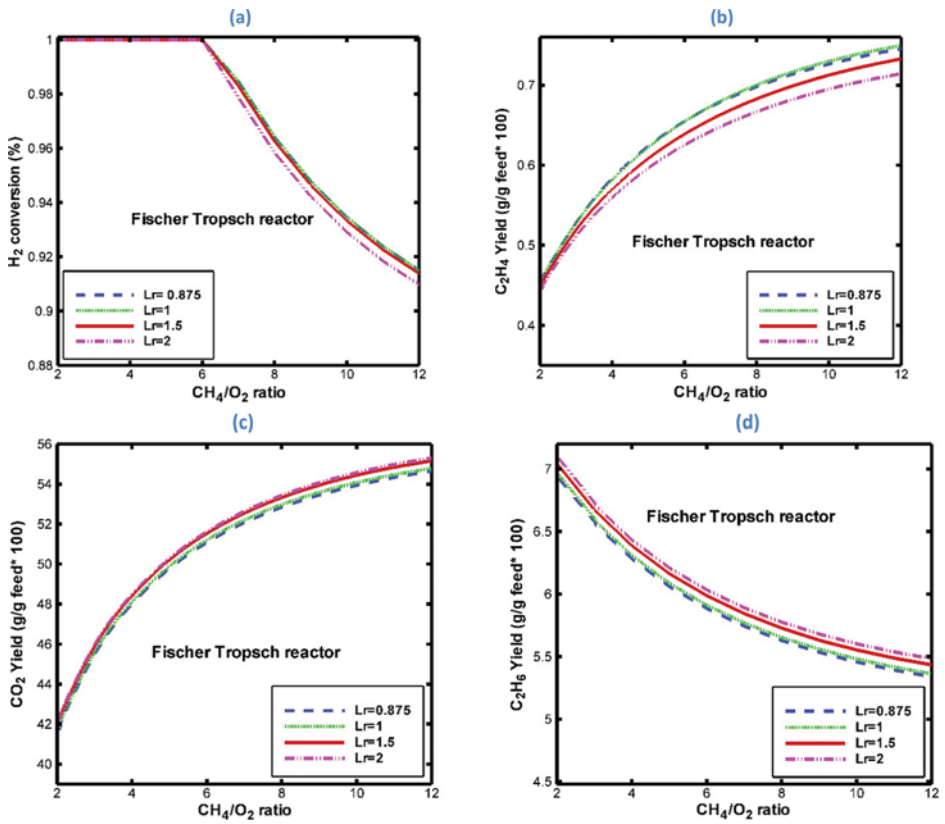

Fig. 16. Comparison of (a) hydrogen conversion (b) C_2H_4 yield (c) CO_2 yield and (d) C_2H_6 yield as a function of L_{ratio} with different CH_4/O_2.

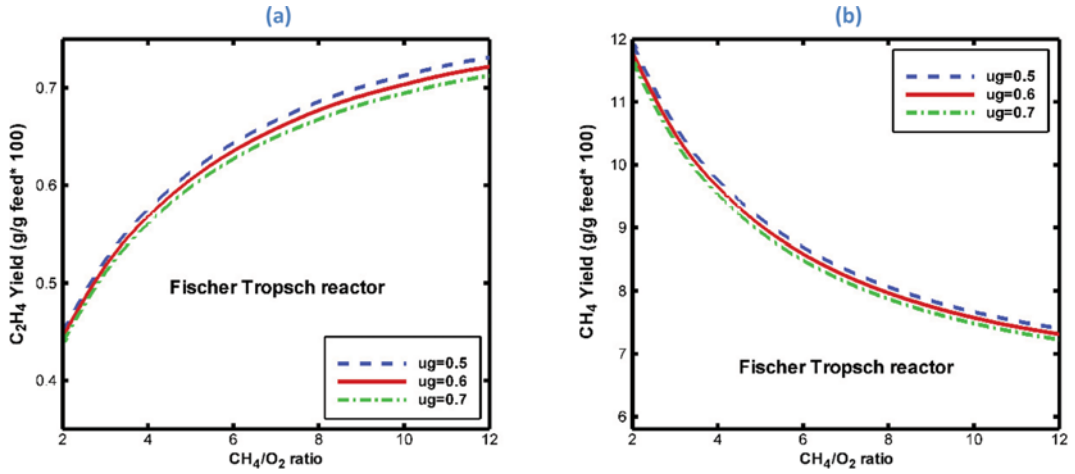

Fig. 17. Effect of gas velocity on (a) C_2H_4 yield and (b) CH_4 yield with input CH_4/O_2 ratio in OCM.

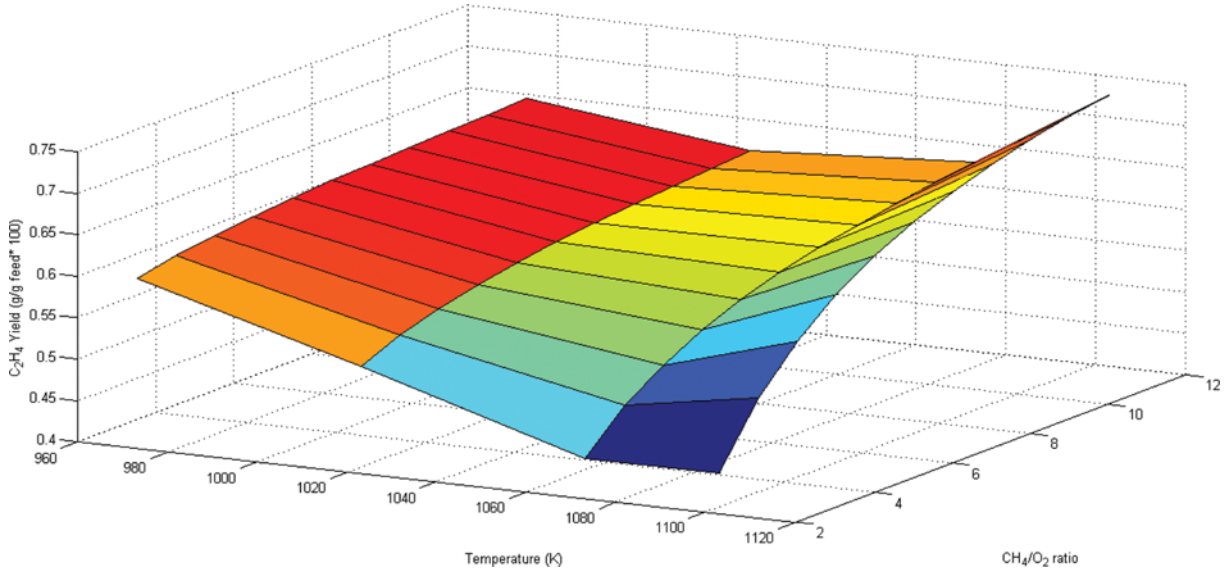

Fig. 18. Three-dimensional profile of ethylene yield in the exit of FR in terms of CH_4/O_2 ratio and temperature of OCM reactor.

tively. As shown in Figs. 16(a) and (b), conversion of H_2 and yield of ethylene at the L_{ratio} of unity is more than other cases. The reason is that the higher the length of membrane fluidized bed reactor, the more CO reaction with hydrogen and more yield of favorable products. Figs. 16(c) and (d) show that yield of CO_2 and ethane at lower L_{ratio} are less than other ratios.

2-9. Effect of Gas Velocity in FT Reactor at Different CH_4/O_2 Ratio

Figs. 17(a) and (b) indicate change of ethylene (as a desired product) and methane (as an undesired product) yield with inlet gas velocity, u_g. Fig. 17 displays that desired FT products increase and undesired FT products decrease with changing u_g from 0.7 to 0.5 m/s, which is the result of more residence time and higher mass transfer coefficient in the fluidized bed. Physical and hydrodynamic parameters such as bubble specifications and overall heat transfer coefficient are the function of gas velocity. Gas velocity variation affects pressure drop and minimum fluidization velocity, too. The pressure drop has the main effect on the partial pressure of components. Since rates of reactions depend on partial pressure, higher pressure drop results in lower reaction rate and products yields. On the other hand, change of minimum fluidization velocity influences bubble diameter (d_b), bubble rising velocity (u_b), volume fraction of bubble phase to overall bed (δ), and mass transfer coefficient between the bubble and emulsion phase (k_{be}).

2-10. Effect of Temperature and CH_4/O_2 Ratio of OCM Reactor

Fig. 18 shows 3D plot of ethylene yield in FT reactor as a function of inlet temperature and CH_4/O_2 ratio of OCM reactor. It can be seen that the C_2H_4 yield increases with CH_4/O_2 ratio of OCM reactor (lower H_2/CO ratio). H_2/CO ratio has considerable influence on the yield of FT product. At low temperature, this ratio is a far from efficient ratio (0.96), but at high temperatures it is near to this ratio (refer to Fig. 6). However, the ethylene yield is less sensitive to temperature at CH_4/O_2=12; ethylene decreases slightly from 973 to 1,073 K and then increases. The same behavior is observed for C_5 yield (Fig. 19).

The results suggest that the concept of FR system is an interesting candidate for application in FT synthesis. However, from an

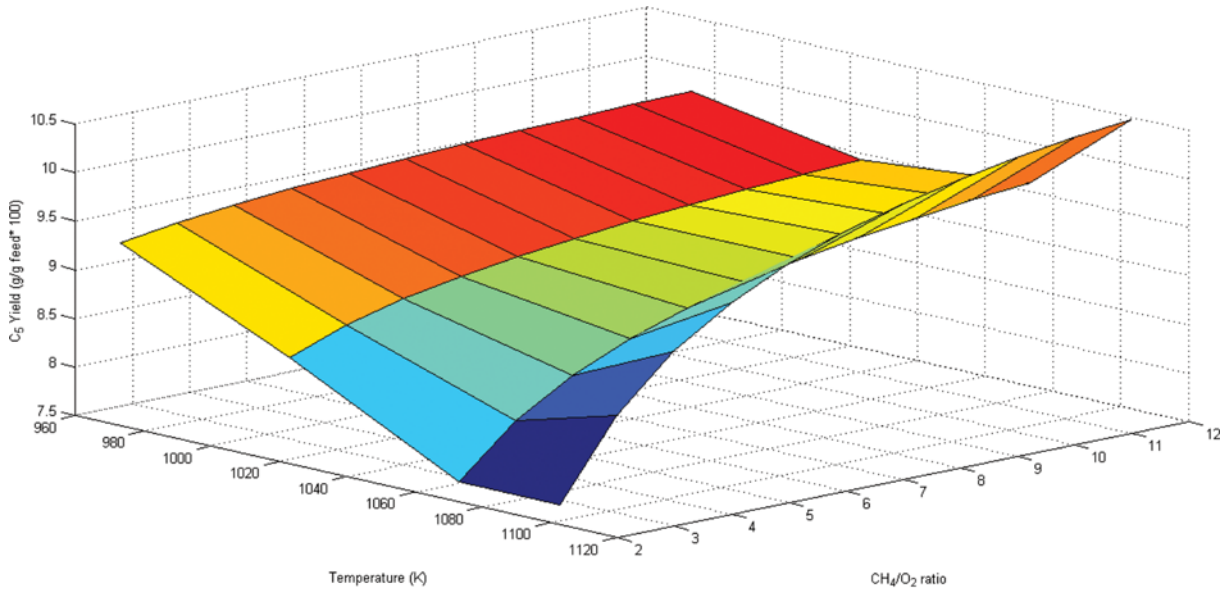

Fig. 19. Three-dimensional profile of C_5 yield of FR in terms of CH_4/O_2 ratio and temperature of OCM reactor.

industrial point of view, there are still many issues to be addressed before putting a case for successful commercialization, such as difficulties in reactor construction, cost of membranes, and sealing in the fluidization conditions. Pd-Ag membrane is mainly used for H_2 separation of relatively simple gas mixture. For an N_2-containing OCM product, Pd-Ag membrane's work condition would meet both the FT process conditions and the OCM products, which include very active ethylene particularly.

CONCLUSIONS

Using consecutive reactors improves the performance of rectors and CH_4 is converted to C_2H_4. The amount of desired components yield in dual type FT reactor is higher than the conventional FT reactor due to diffusion of hydrogen to the reaction side and increasing the conversion of CO. Another useful concept of dual type FT reactor is decreasing the amount of CH_4 and CO_2 as undesired by-products of FT reaction. This reactor configuration can be suggested to produce more desirable hydrocarbons. Although the results are very interesting and thus can be taken as reference for future research activities, the main problem is the practical section of work and the proposed process configuration, which is too complicated. However, future development will reduce these problems.

NOMENCLATURE

A_c : cross-section area of tube [m^2]
A_i : inner area of each tube [m^2]
A_s : lateral area of each tube [m^2]
A_{shell} : cross-section area of shell [m^2]
a_b : interface between bubbles and emulsion [m^2]
a_v : specific surface area of catalyst pellet [$m^2 \cdot m^{-3}$]
c_p : specific heat [$kJ \cdot mol^{-1} \cdot K$]
c_{Pg} : specific heat of the gas at constant pressure [$J \cdot mol^{-1} \cdot k^{-1}$]
c_{Ph} : specific heat of the hydrogen at constant pressure [$J \cdot mol^{-1} \cdot k^{-1}$]
c_{Ps} : specific heat of the catalyst at constant pressure [$J \cdot mol^{-1} \cdot k^{-1}$]
C_t : total concentration [$mol \cdot m^{-3}$]
C_j : concentration of species j [$mol \cdot m^{-3}$]
c_{Ph} : specific heat of hydrogen at constant pressure [$Jmol^{-1}K^{-1}$]
d_t : tube diameter [m]
d_p : pellet diameter [m]
D_i : Tube's inside diameter [m]
D_o : Tube's outside diameter [m]
D_{ij} : binary diffusion coefficient of component i in j [$m^2 \cdot s^{-1}$]
D_m^i : diffusion coefficient of component i in the mixture [$m^2 \cdot s^{-1}$]
D_{ro} : Reaction's outside diameter [m]
d_p : particle diameter [m]
F_t : total molar rate for shell side [$mol \cdot s^{-1}$]
h_f : gas-catalyst's heat transfer coefficient [$W \cdot m^{-2} \cdot K^{-1}$]
h_i : heat transfer coefficient between fluid phase and reactor wall [$W \cdot m^{-2} \cdot K^{-1}$]
h_o : heat transfer coefficient between coolant stream and reactor wall [$W \cdot m^{-2} \cdot K^{-1}$]
F_t : total molar rate for shell side [$Mol \cdot s^{-1}$]
ΔH_{rij} : heat of reaction [$kJmol^{-1}$]
K : conductivity of fluid phase [$W \cdot m^{-1} \cdot K^{-1}$]
K_w : thermal conductivity of reactor wall [$W \cdot m^{-1} \cdot K^{-1}$]
k_{gi} : mass transfer coefficient between gas and solid phase for component i [$m \cdot s^{-1}$]
k_{bei} : mass transfer coefficient between bubble and emulsion phase for component i [$m \cdot s^{-1}$]
L : length of reactor [m]
M_i : molecular weight of component i [$g \cdot mol^{-1}$]
N : number of components [-]
P total pressure [bar]
P_a : atmospheric pressure [bar]

p_H^{sh} : shell-side pressure [bar]
p_H^t : tube-side pressure [bar]
$\overline{P}$: permeability of hydrogen through Pd-Ag layer [mol m^{-1} s^{-1} $pa^{-1/2}$]
P_0 : pre-exponential factor of hydrogen permeability [mol m^{-1} $s^{-1}Pa^{-1}$]
$r_{c,j}$: rate of formation of catalytic reaction j [mol g^{-1} s]
$r_{g,i}$: rate of formation of gas-phase reaction j [mol g^{-1} s]
R_i : inner radius of Pd-Ag layer [m]
R_o : outer radius of Pd-Ag layer [m]
Re : Reynolds number
T : temperature [K]
T_{ex} : external temperature [K]
T_{shell} : temperature of coolant stream in fixed bed reactor [K]
u_s : superficial velocity [ms^{-1}]
U : overall heat transfer coefficient [Wm^{-2} K]
U_{shell} : overall heat transfer coefficient between coolant and process streams [$W \cdot m^{-2} \cdot K^{-1}$]
y_i : mole fraction of component i in the fluid phase [$mol \cdot mol^{-1}$]
y_{is} : mole fraction of component i in the solid phase [$mol \cdot mol^{-1}$]
y_{ie} : mole fraction of component i in the emulsion phase [$mol \cdot mol^{-1}$]
y_{ib} : mole fraction of component i in the bubble phase [$mol \cdot mol^{-1}$]
Z : axial reactor coordinate [m]

Greek Letters

ε_b : porosity of catalyst bed
ρ_b : density of catalyst in the bed [$g \cdot m^{-3}$]
ρ_g : density of system gas [kgm^{-3}]
α_H : hydrogen permeation rate constant [mol m^{-1} s^{-1} $Pa^{-0.5}$]
η : catalyst effectiveness factor
Ψ : shape factor
$\Delta H_{f,i}$: enthalpy of formation of component i [$J \cdot mol^{-1}$]
ΔH_{298} : enthalpy of reaction at 298 K [$J \cdot mol^{-1}$]
δ : bubble phase fraction
ε_B : void fraction of catalytic bed [-]
ε_s : void fraction of catalyst [-]
ε_{mf} : void fraction of bed at minimum fluidization [-]
y : volume fraction of catalyst occupied by solid particles in bubble [-]

REFERENCES

1. G. E. Keller and M. M. Bhasin, *J. Catal.*, **73**, 9 (1982).
2. Y. San Su, J. Y. Ying and W. H. Green, *J. Catal.*, **218**, 321 (2003).
3. S. Stünkel, W. Martini, H. Arellano-Garcia and G. Wozny, *Chem. Ing. Technol.*, **83**, 488 (2011).
4. S. Arndt, G. Laugel, S. Levchenko, R. Horn, M. Baerns, M. Scheffler, R. Schlögl and R. Schomäcker, *Catal. Rev.*, **53**, 424 (2011).
5. M. Y. Sinev, Z. T. Fattakhova, V. I. Lomonosov and Y. A. Gordienko, *J. Nat. Gas. Chem.*, **18**, 273 (2009).
6. M. R. Ehsani, H. Bateni and G. R. Parchikolaei, *Korean J. Chem. Eng.*, **29**, 855 (2012).
7. M. R. Lee, M. J. Park, W. Jeon, J. W. Choi, Y. W. Suh and D. J. Suh, *Korean J. Chem. Eng.*, **28**, 2142 (2011).
8. H. R. Godini, S. Xiao, M. Kim, N. Holst, S. Jašo, O. Görke, J. Steinbach and G. Wozny, *J. Ind. Eng. Chem.*, **20**, 1993 (2014).
9. M. A. Marvast, M. Sohrabi, S. Zarrinpashneh and G. H. Baghmisheh, *Chem. Eng. Technol.*, **28**, 78 (2005).
10. A. Ghareghashi, S. Ghader and H. Hashemipour, *J. Ind. Eng. Chem.*, **19**, 1811 (2013).
11. N. Park, J. R. Kim, Y. Yoo, J. Lee and M. J. Park, *Fuel*, **122**, 229 (2014).
12. N. Moazami, M. L. Wyszynski, H. Mahmoudi, A. Tsolakis, Z. Zou, P. Panahifar and K. Rahbar, *Fuel*, **154**, 140 (2015).
13. Z. Stansch, L. Mleczko and M. Baerns, *Ind. Eng. Chem. Res.*, **36**, 2568 (1997).
14. M. Rahmati, M. Mehdi and M. Bargah-Soleimani, *Can. J. Chem. Eng.*, **79**, 800 (2001).
15. Fischer-Tropsch pilot plant of Research Institute of Petroleum Industry and National Iranian Oil Company, Iran (2004).
16. E. L. Cussler, "Diffusion, Mass Transfer in Fluid Systems," Cambridge: Cambridge University Press, 525, II (1984).
17. C. R. Wilke, *Chem. Eng. Progress*, **45**, 218 (1949).
18. M. Panahi, Master's Thesis, Sharif University of Technology (2005).
19. M. R. Rahimpour and M. Lotfinejad, *Chem. Eng. Technol.*, **31**, 38 (2008).
20. M. R. Rahimpour, A. Khosravanipour Mostafazadeh and M. M. Barmaki, *Fuel. Process. Technol.*, **89**, 1396 (2008).
21. F. Guazzone, E. E. Engwall and Y. H. Ma, *Catal. Today*, **118**, 24 (2006).
22. S. Deshmukh, J. A. Laverman, A. H. G. Cents, M. van Sint Annaland and J. A. M. Kuipers, *Ind. Eng. Chem. Res.*, **44**, 5955 (2005).
23. J. Chang, L. Bai, B. Teng, R. Zhang, J. Yang, Y. Xu, H. Xiang and Y. Li, *Chem. Eng. Sci.*, **62**, 4983 (2007).
24. D. Kunii and O. Levenspiel, Fluidization Engineering, Butterworth-Heinemann, Boston (1991).
25. J. Ghajar, Master's Thesis, Shiraz University, Department of Chemical and Petroleum Engineering (2000).